Visualization of boiling FC-72 on plate heat exchanger

Kenta Hayashi*, Hirofumi ARIMA**, Takuya Tanaka***
*Graduate school of Sci. Eng., Saga Univ.
1-Honjo, Saga-shi, Saga 840-8502, Japan
Email: 21728011@edu.cc.saga-u.ac.jp
**Institute of Ocean Energy, Saga Univ., 1-48, Hirao, Kubara-aza, Yamashiro-cho, Imari-shi, Saga, 849-4256, Japan
***Faculty of Sci. Eng., Saga Univ., 1-Honjo, Saga-shi, Saga 840-8502, Japan

Abstract

To improve the performance of the plate heat exchanger for OTEC, visualization was performed to confirm the boiling behaver inside the plate heat exchanger. The anodic oxidation aluminum heat plate has been adopted as a heat exchange plate. However, there are no adoption of the anodic oxidation aluminum plate for the plate heat exchanger. In this experiment, flow boiling was visualized using FC-72 as the working fluid using a newly adopted aluminum plate and a plate heat exchanger with a visualization window, which is an improved frame of the plate heat exchanger. The heat transfer surfaces used in the experiments were a smooth surface and a herringbone surface, both of which were anodized aluminum plates. It is intended for use with ammonia and is coated for corrosion resistance. In this experiment, the experimental conditions are mass flux G (10, 20, 30, 40kg/m^{2}s), volumetric flow rate of hot water m_{hw} (2.5, 5, 7.5, 10L/min), degree of subcooling of working fluid ΔT_{sub} (0, 5, 10K), and the boiling phase was taken a video with a high-speed camera. From this experiment, the following things were found. In case of the flow rate of hot water increases, the amount of bubbles nucleation increases and the size of the bubbles increases. The void fraction distribution in the flow direction was obtained by visualization image analysis. The heat transfer coefficient increased with the increase of quality x. At $x > 0.8$, the heat transfer coefficient was decreased due to dry-out was observed. It was also confirmed that the heat transfer coefficient of the working fluid increases as the mass flux of the working fluid increases.

KeyWords : Boiling, Visualization, Herringbone plate, Anodic Oxidation Aluminum, FC-72

1. Introduction

In order to improve the performance of plate evaporators for ocean thermal energy conversion, it is essential to clarify the boiling heat transfer characteristics of plate evaporators. Among them, we have conducted visualization observations to clarify the boiling behavior in plate heat exchangers. In this study, a sight glass was installed in the plate-type evaporator frame in order to obtain a wide visualization area. Visualization experiments was performed using it. Boiling heat transfer was measured and the boiling behaver was visualized.

2. Experiment

2.1 Experimental apparatus

The experiment was a forced convection boiling experiment of FC-72. Fig. 1 shows that the schematic diagram of experimental apparatus. The experimental apparatus consists of a test section (plate heat exchanger), a hot water tank, a hot water pump, a working fluid tank, a working fluid pump and a preheater. In addition, the equipment has two circulation cycles: a working fluid and a hot water circulation system. The test section has a visualization sight glass on the frame of plate heat exchanger. In addition, the working fluid pump is a magnet pump, the hot water pump is also a magnet pump. The hot water tank consists of a stainless-steel tank and immersion heaters. The pre-heater has a structure in which a ribbon heater is wrapped around the surface of a copper tube.

State quantities were measured with various sensors. The temperature was measured with a K-type thermocouple, the working fluid flow rate was measured with Coriolis mass flowmeter and volumetric flow rate of hot water was measured with magnetic flowmeter. These values measured by each sensor were collected and recorded in a data logger.

Fig. 2 shows a schematic diagram of the test section, and Fig. 3 shows the test plates. This test plate is surface-treated by anodic oxidation specified in JIS H8601 in order to provide corrosion resistance. Also, the film thickness is equivalent

to AA15 (20 to 25 μm by actual measurement). Table 1 shows the experimental conditions of this experiment.

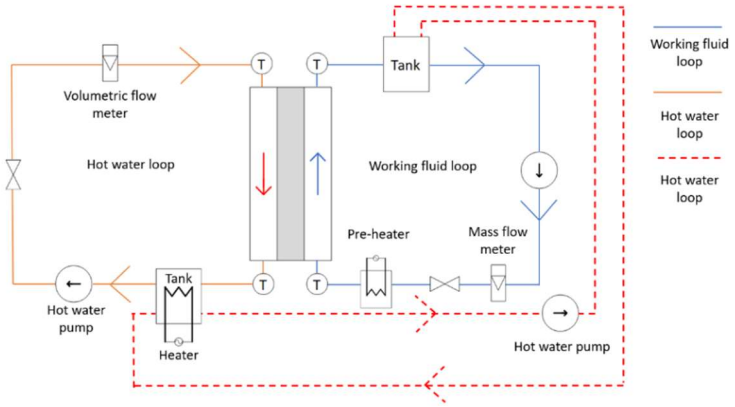

Fig. 1 Schematic diagram of experimental apparatus.

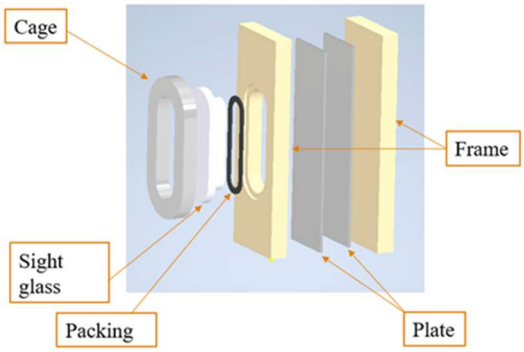

Fig. 2 Assembly of test section.

(a) Smooth plate

(b) Herringbone plate

Fig.3 Test plates.

Table 1 Experimental conditions.

Mass flux of working fluid G [kg/m^{2}s]	10, 20, 30, 40
Volumetric flow rate of hot water m_{hw} [L/min]	2.5, 5, 7.5, 10
Degree of subcooling of working fluid ΔT_{sub} [K]	0, 5, 10

2.2 Data reduction

The overall heat transfer coefficient U, boiling heat transfer coefficient h_{wf}, pressure drop ΔP_{fr}, and duct friction coefficient f_{tp} were obtained. These values were calculated by following equations:

$$U = \frac{Q}{A\Delta T_{lm}} \quad (1)$$

$$h_{wf} = 1/(\frac{1}{U} - \frac{1}{h_{hw}} - \frac{t}{k}) \quad (2)$$

$$\Delta P_{fr} = \Delta P_{tot} - \Delta P_a - \Delta P_{man} - \Delta P_{ele} \quad (3)$$

$$f_{tp} = \Delta P_{fr} \left(\frac{D_h}{L}\right)\left(\frac{\rho_m}{2G^2}\right) \quad (4)$$

2.3 Procedure of visualization

The boiling behavers were visualized by the following method. A high-speed camera was arranged in front of the sight glass. A cold lamp was arranged in front of the sight glass as a light source. The visualization movie was recoded period of 2 seconds at the frame rate (2000 fps) and resolution (1280 × 1028 pixels).

2.4 Analysis visualization data

Visualization data was analyzed by the following method. According to a two seconds length visualization movie was divided into each frame, 2000 image files were made. An image file was analyzed by developed software. In the image analysis, the distribution of bubbles in an image file was extracted by using HOG method with machine learning. The

void fraction was calculated based on the bubble distribution.

3. Result and discussion

3.1 Experiment of visualization

Fig 4 and 5 show visualized images obtained in the experiment. According to Fig. 4, at the flat plate, in case of the mass flux of the working fluid and the degree of subcooling are same condition, the amount of bubbles nucleation and the size of the bubbles increases with an increase in the volumetric flow rate of hot water.

According to Fig. 5 at the herringbone plate, it can be shown that in case of the mass flux of the working fluid and the degree of subcooling are equal, the amount of bubbles nucleation and the size of the bubbles also increases with an increase in the volumetric flow rate of hot water increases with an increase in the volumetric flow rate of hot water.

(a) G = 20 kg/m²s
m_{hw} = 2.5 L/min
ΔT_{sub} =10 K

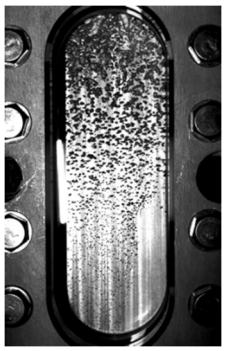

(b) G = 20 kg/m²s
m_{hw} = 5 L/min
ΔT_{sub} =10 K

(c) G = 20 kg/m²s
m_{hw} = 10 L/min
ΔT_{sub} =10 K

Fig. 4 Comparison of boiling phenomenon at different flow rate of hot water on flat plates.

(a) G = 10 kg/m²s
m_{hw} = 2.5 L/min
ΔT_{sub} = 0K

(b) G = 10 kg/m²s
m_{hw} = 3.9 L/min
ΔT_{sub} = 0K

Fig. 5 Comparison of boiling phenomenon at different flow rate of hot water on herringbone plates.

3.2 Analyzed visualization data

The visualized image obtained by the visualization experiment was analyzed with developed software (Tanaka 2021), and the bubble distribution on the heat transfer surface was obtained. The results are shown in Fig. 6 (a) and (b). Fig 6 (a) and (b) are the results obtained at different mass fluxes ((a) G = 20 kg/m²s, (b) G = 40 kg/m²s). (1) and (2) in Fig.6 (a) and (b) are the original image (1) obtained by visualization, and the bubble distribution image (2) obtained by image analysis.

In Fig. 6(a)-(1), there are almost no bubbles near the working fluid inlet at the bottom right of the image. On the other hand, bubbles originate from the lower left area. Furthermore, as the bubbles rise to the top of the figure, their diameter increases and they coalesce. In the lower right region, no bubbles were observed because the working fluid was supercooled. In addition, the working fluid is subcooled in the lower left region, which coincides with the hot water side exit across the heat transfer surface. As shown in Fig. 6(a)-(2), these differences can be clearly seen as differences in bubble distribution between the lower right region and the lower left region by image processing.

On the other hand, under the condition of Fig. 6(b) where the mass flux is large, the distribution of bubbles can be seen over the entire area as shown in Fig. 6(b)-(1). Also, at the inlet, the bubble diameter is generally larger than his Fig. 6(a) condition. Since the mass flux is larger in Fig. 6(b), the quality at the plate exit is smaller and the distribution of bubbles is thought to be smaller. From this, as can be seen in Fig. 6(a), there is almost no difference the bubbles distribution between right and left area at the bottom of the plate. The reason of that the bubbles are distributed over the entire heat transfer surface. Incidentally, the image analysis results are shown in Fig. 6(b)-(2), and bubbles weren't detected in the lower left area. The reason is that the image analysis program using machine learning misidentified bubbles as noise.

Fig. 7 compares the void fraction distribution in the flow direction under the conditions of Fig. 6(a) and (b). The void fraction distribution in Fig. 6(a) showed a tendency to increase sharply from near the center of the heat transfer surface in the height direction (x = 150 mm). On the other hand, the void fraction distribution in Fig. 6(b) was almost constant over the entire heat transfer surface.

3.3 Measurement of overall and boiling heat transfer coefficient

Fig. 8 shows the overall heat transfer coefficient against to the hot water flow velocity. Both smooth and herringbone

surfaces showed a decrease in overall heat transfer coefficient with an increasing in hot water flow velocity. In addition, Fig. 9 shows heat transfer coefficient against to the outlet quality. In both cases, it can be seen that at the higher the quality, the higher the heat transfer coefficient were observed.

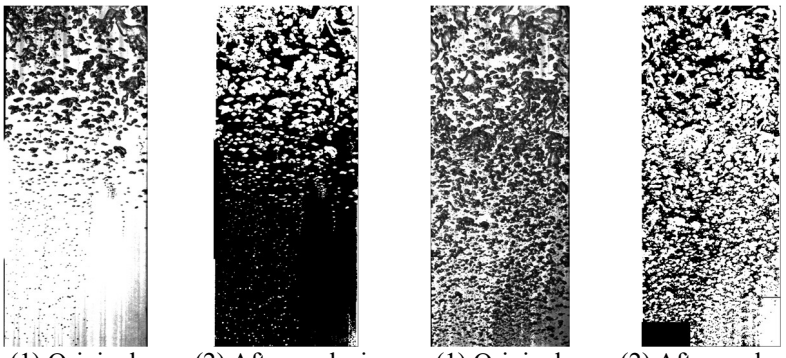

(a) Run 1 (G = 20 kg/m²s, m_{hw} = 2.5 L/min, ΔT_{sub} =10 K)

(b) Run 2 (G = 40 kg/m²s, m_{hw} = 2.5 L/min, ΔT_{sub} = 5 K)

Fig. 6 Analysis of boiling phenomenon.

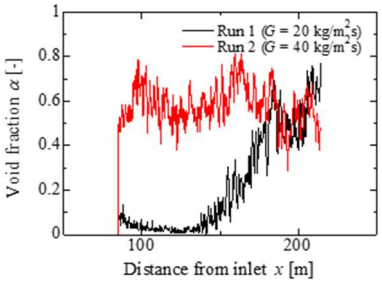

Fig. 7 Distributions of void fraction against flow direction at different mass flux of working fluid.

(a) Smooth surface plate, ΔT_{sub} = 0

(b) Herringbone plate, ΔT_{sub} = 0

Fig. 8 Overall heat transfers against hot water flow velocity.

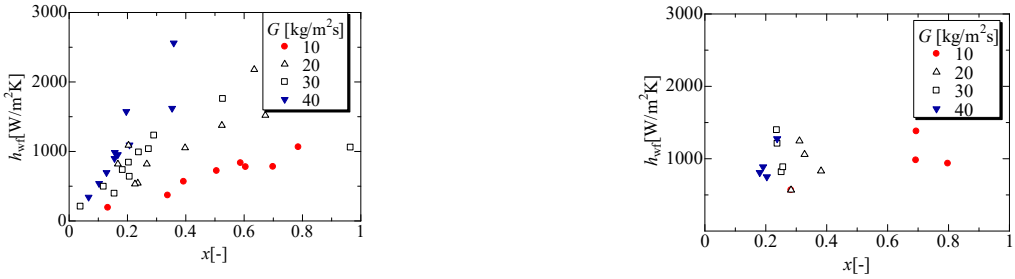

(a) Smooth surface plate

(b) Herringbone plate

Fig. 9 Heat transfer coefficients of FC-72 against vapor quality.

4. Conclusion

(1) As increasing the hot water flow rate, the amount of bubbles nucleation the size of the bubbles increases.

(2) The void fraction distribution in the flow direction was obtained by visualization image analysis.

(3) The heat transfer coefficient increased with the increase in quality x. At x > 0.8, the heat transfer coefficient was decreasing due to dry-out.

(4) It was also confirmed that the heat transfer coefficient of the working fluid increases as the mass flux of the working fluid increases.

References

Takuya Tanaka, Analysis of visualization image of boiling behaver on plate heat exchanger using machine learning, Thesis of under graduate school, Faculty of Sci. Eng., Saga Univ (2021).